



Evaluation of Pulmonary Effects of 3-D Printer Emissions From Acrylonitrile Butadiene Styrene Using an Air-Liquid Interface Model of Primary Normal Human-Derived Bronchial Epithelial Cells

International Journal of Toxicology
2022, Vol. 41(4) 312–328
© The Author(s) 2022
Article reuse guidelines:
sagepub.com/journals-permissions
DOI: 10.1177/10915818221093605
journals.sagepub.com/home/ijt


Mariana T. Farcas^{1,2}, Walter McKinney¹, Jayme Coyle¹, Marlene Orandle¹, W. Kyle Mandler¹, Aleksandr B. Stefaniak^{1,3}, Lauren Bowers^{1,3}, Lori Battelli¹, Diana Richardson¹, Mary A. Hammer¹, Sherri A. Friend¹, Samantha Service¹, Michael Kashon¹, Chaolong Qi⁴, Duane R. Hammond⁴, Treye A. Thomas³, Joanna Matheson⁵, and Yong Qian¹ 

Abstract

This study investigated the inhalation toxicity of the emissions from 3-D printing with acrylonitrile butadiene styrene (ABS) filament using an air-liquid interface (ALI) *in vitro* model. Primary normal human-derived bronchial epithelial cells (NHBEs) were exposed to ABS filament emissions in an ALI for 4 hours. The mean and mode diameters of ABS emitted particles in the medium were 175 ± 24 and 153 ± 15 nm, respectively. The average particle deposition per surface area of the epithelium was $2.29 \times 10^7 \pm 1.47 \times 10^7$ particle/cm², equivalent to an estimated average particle mass of 0.144 ± 0.042 µg/cm². Results showed exposure of NHBEs to ABS emissions did not significantly affect epithelium integrity, ciliation, mucus production, nor induce cytotoxicity. At 24 hours after the exposure, significant increases in the pro-inflammatory markers IL-12p70, IL-13, IL-15, IFN-γ, TNF-α, IL-17A, VEGF, MCP-1, and MIP-1α were noted in the basolateral cell culture medium of ABS-exposed cells compared to non-exposed chamber control cells. Results obtained from this study correspond with those from our previous *in vivo* studies, indicating that the increase in inflammatory mediators occur without associated membrane damage. The combination of the exposure chamber and the ALI-based model is promising for assessing 3-D printer emission-induced toxicity.

Keywords

3-D printer, printer emitted nanoparticles, thermoplastics, acrylonitrile butadiene styrene, filament, air-liquid interface, *in vitro*, human bronchial epithelial cells

Introduction

An accelerating expansion and evolution of fused filament fabrication (FFF), a three-dimensional (3-D) printing process, is occurring across industries. Considerable evidence¹⁻¹⁹ shows that the FFF 3-D printing process releases a significant number of nanoparticles (NPs; diameter <100 nm) that can deposit deep in the lower respiratory tract and may cause adverse respiratory effects. The FFF 3-D printing process also releases various volatile organic compounds (VOCs) during printing, which might pose serious risk concerns to human health as they are known irritants, carcinogens, odorants, and reprotoxins.²⁰ VOCs exposure can occur through gas phase substances as well as via particle-adhered VOCs.

¹Health Effects Laboratory Division, National Institute for Occupational Safety and Health, Morgantown, WV, USA

²Department of Pharmaceutical and Pharmacological Sciences, School of Pharmacy, West Virginia University, Morgantown, WV, USA

³Respiratory Health Division, National Institute for Occupational Safety and Health, Morgantown, WV, USA

⁴Division of Field Studies and Engineering, National Institute for Occupational Safety and Health, Cincinnati, OH, USA

⁵Office of Hazard Identification and Reduction, U.S. Consumer Product Safety Commission, Rockville, MD, USA

Corresponding Author:

Yong Qian, Pathology and Physiology Branch, Health Effects Laboratory Division, National Institute for Occupational Safety and Health, 1095 Willowdale Road, Morgantown, WV 26505, Washington 20201, DC, USA. Email: yaq2@cdc.gov

The potential toxicity of aerosolized emissions from 3-D printers has been tested in conventional submerged single-cell culture^{21,22} and animal models.^{21,23,24} However, submerged cultured cell *in vitro* models, used for performing cytotoxicity assessment of the respiratory system, have several drawbacks. These models do not mimic *in vivo* conditions such as the morphological and physiological features of airway mucosa characterized by the presence of ciliated columnar cells, mucous-producing goblet cells, and basal cells.²⁵ Furthermore, the addition of test agents in liquid form directly into the cell culture medium may alter the test substance's physicochemical properties (e.g. size, surface charge, solubility, transformation, or agglomeration state), leading to unreliable outcomes or inaccurate dose-response.²⁶ In addition, there is an inability to recapitulate the physiological inhalation conditions and aerosol deposition patterns compared to the *in vivo* human exposures.²⁶ Rodent models have been routinely used in experimental toxicology and risk/hazard assessments. However, data extrapolation from animals to humans is challenging because of respiratory tract interspecies variability. Such differences include: (1) respiratory tract architectural features (eg, nasal cavity gross anatomy, airway structure, and branching pattern, the number of cartilaginous airways, cell types, and composition within the regions of the respiratory tract); (2) respiratory physiology (eg, breathing mode and ventilatory patterns, metabolic rates); and (3) biochemistry (eg, composition and biotransformation capacity of P450 monooxygenases, epoxide hydrolase and glutathione S-transferase).²⁷⁻³¹ These variations likely influence the local toxic effects due to differences in the airflow pattern in the respective respiratory tract architecture, which affects the deposition of the given inhaled test agents as well as their retention and clearance from the lungs.³² Moreover, studies of translational toxicology from rodents to humans used in setting occupational exposure limits for hazard classification found that the extrapolation and standardization of rat lung mass or rat body weight to humans is varying and inconsistent,³³ and the genomic responses in mouse models poorly mimic human inflammatory diseases.³⁴ These animal and single cell *in vitro* model limitations have led to the development of human-relevant toxicity research models, with particular emphasis on *in vitro* systems.^{26,35,36}

Physiologically relevant respiratory epithelium models, such as *in vivo*-like *in vitro* models cultured at the air-liquid interface (ALI), are routinely used to study inhaled particles- or gases-mediated respiratory toxicity.³⁷ These methods are promising in the domain of inhalation toxicology as they more closely mimic the *in vivo* respiratory epithelium in its organization and stratification, thus avoiding limitations posed by the submerged monolayer cultures. This three-dimensional (3D) *in vitro* tissue model consists of normal, human-derived bronchial epithelial cells (NHBEs) cultured on porous membranes, resulting in a polarized, fully differentiated airway epithelial cell layer. This *in vitro* epithelium is predominantly composed of three cell types, including

mucus-producing goblet cells (secretory cells), ciliated respiratory epithelial cells, and basal cells (progenitor cells). This architecture mimics the *in vivo* respiratory tract by modeling epithelial barrier function (eg, development of high trans-epithelial electrical resistance, expression and functionality of tight junctions, and paracellular permeability), mucous production, and cilia function. Furthermore, the suitability of ALI cultures as a benchmark for a human-relevant model is further confirmed through transcriptome analyses,³⁸ with several reports demonstrating physiological responses to toxicants or pathogens.³⁹⁻⁴³ Moreover, the ALI approaches have been used as an alternative in some animal-based inhalation toxicity studies.⁴⁴

Given that there are numerous types of feedstock filaments on the market and the physicochemical characteristics of FFF 3-D printing emissions vary with each individual filament type,^{45,46} these factors might suggest that the potential toxic effects they pose may vary with filament type as well. Thus, ALI culture models provide a unique *in vitro* high throughput platform to assess the exposure to 3-D printer emissions, avoiding the drawbacks of using submerged single cell *in vitro* models, and animal models and would likely reduce the time and expenses of traditional *in vivo* toxicity testing and screening of multiple filaments at once.

This study investigated the use of primary NHBEs in ALI cell culture as an *in vitro* inhalation toxicity model of lung epithelium to the effects of 3-D emissions upon airway epithelial cells. We evaluated cytotoxicity, tissue injury, and inflammatory and immune system regulation markers following exposure to blue colored ABS filament (3DXTECH, Byron Center, MI), one of the most common commercial filaments. The most common feedstock filaments for 3-D printing are ABS and polylactic acid (PLA), holding approximately 29 and 42% market share, respectively.⁴⁷ While ABS holds less market share, it is a petroleum-based polymer and it is generally accepted that it emits more particles compared with PLA, so it was chosen for this study. ABS filament contains styrene which is also a health concern if inhaled.

Materials and Methods

Cell Culture Model

Primary NHBEs, isolated from the epithelium of human bronchi, were purchased from PromoCell (cat. C-12640, PromoCell GmbH, Germany). Cryopreserved cells (healthy donor number 446Z036.9 and 432Z016.5; viability $\geq 94\%$; 500,000 cells per vial) were cultured and differentiated according to the manufacturer's instructions. Briefly, cells (passage P+1) were expanded in one T75 Corning™ Cell Culture Treated Flask, using the Pneumacult-Ex Plus expansion medium (cat. 05040, Stemcell Technologies, Vancouver, Canada), supplemented with 0.1% (v/v) hydrocortisone (cat. 07925, Stemcell Technologies). NHBE

were cultured at 37°C and under 5% CO₂ in air conditions, with a medium change every other day. After reaching 70% confluency, the cells were passaged into four T75 Corning™ Cell Culture Treated Flasks (cell density at 0.5×10^4 cells/cm²) using an Animal Component-Free Cell Dissociation Kit (Stemcell Technologies) for 7-10 minutes at 37°C. The detached cells (passage P+2) were centrifuged at 350 g for 5 minute and re-suspended in the expansion medium. Cells were cultured for additional 4-5 days in the expansion medium, with medium changed every other day, and subsequently used for the ALI procedure. To proceed with the ALI, 0.12×10^6 cells in 0.5 mL PneumaCult™-Ex Plus Medium were seeded on the apical side of inserts (0.4 µm pore membrane, Polyester, Costar® 12 mm Transwell®, Stemcell Technologies) in a 12-well plate with 1 mL expansion medium added into the basolateral chamber. The ALI condition was initiated 5 days post-seeding by the complete aspiration of the expansion medium in the apical compartment, thereby exposing the epithelial cells to the atmosphere (day 0 post-ALI) and replacing the medium from the basal compartment with the PneumaCult™-ALI Maintenance Medium (ALI medium). The ALI medium consisted of PneumaCult™-ALI Basal Medium containing 10% (v/v) PneumaCult™-ALI 10X Supplement, 1% (v/v) PneumaCult™-ALI Maintenance Supplement, 0.2% (v/v) heparin solution, 0.5% (v/v) hydrocortisone and 1% (v/v) penicillin/streptomycin. The cells were fed from the basal compartment with fresh ALI medium and maintained for 23 days before exposure to 3-D printer emissions.

Air-Liquid Interface Cell Exposure

Exposure System. The differentiated NHBEs cells were exposed to ABS 3-D printer emissions at the ALI using the same exposure system utilized previously to expose Sprague-Dawley rats to emissions generated during real-time printing via a whole-body inhalation exposure system. The 3-D printer emission characterization and exposure chamber system are described in detail in our previous study.²⁴ In brief, this system housed three 3D printers (Lulzbot mini, FAME 3d, Fargo, ND) inside a fume generation chamber. The emissions from the printers were delivered to an exposure chamber (150L volume) at a flow rate of 25 L/min. Particle count concentration, mass concentration, temperature, humidity, and CO₂ levels were monitored inside the exposure chamber and recorded in real time by the system software. Blue colored ABS filament (3DXTECH, Byron Center, MI), was used for all exposures. The object printed was a block; 12.7 cm wide by 12.7 cm long with a height of 2.54 cm. When not in use the filament was stored at room temperature in an airtight dry box. Supplemental Table 1 details the 3-D printer settings used during all exposures. Cell wells were placed inside the exposure chamber therefore diffusion and settling would be the primary factors for particle deposition onto the cells. A

fresh supply of 25 L/min of particles and fume was supplied to the chamber during all exposures. The average mass concentration inside the exposure chamber was 250 µg/m³, and the average count concentration was approximately 200,000 particles per cm³.

Cell Exposure Treatment. Before the cell exposure treatment, cell morphology was inspected using phase-contrast microscopy (Supplemental Figure 1 Phase Contrast Images of Cells at ALI) followed by transepithelial electrical resistance (TEER) measurements, as described in the next paragraph.

Four different sets of treatments were employed as follows: (1) cell inserts were placed in the middle of the exposure chamber and exposed for 4 hours to the ABS FFF 3-D printer emissions (marked as ABS-exposed cells); (2) another set of cells on inserts were kept inside the emissions chamber covered, serving as exposure chamber negative controls (marked as “exposure chamber” samples); (3) a third set of cells were maintained in the incubator at normal growing conditions, serving as incubator controls (marked as “incubator” samples); and (4) the last set of cells were treated on the apical surface of epithelial tissue with 0.1 mL 2% Triton X-100 (TX-100) (1 hour prior to when the exposure ended) to serve as a positive control for cytotoxicity and disruption of barrier integrity. After the 4 hour exposure treatment (time 0 hour) and 24 hour post-exposure, various endpoints were evaluated, including changes in phenotypic characteristics (presence of ciliated, goblet, and basal cells), functional changes, cytotoxicity, and inflammatory and immune system regulation markers (cytokines, chemokines, and growth factors). To determine if the exposure system might be a source of contamination, a plate containing cell culture medium without antibiotics was kept open in the exposure chamber during the 4 hour exposure. This plate was maintained in the incubator for 2 weeks, inspected for contamination visually as well as by trypan blue stain. After 2 weeks, the media was clear and no contamination was observed, and no cells were present in the trypan blue-stained suspension. Studies were performed in single independent experiments with N = 1-3 inserts/treatment, n = 2-3 replicates each.

Deposition Characterization. During the 4 hour exposure to ABS emissions (250 µg/m³), a 12-well Costar® Transwell® plate containing 0.5 mL PneumaCult™-Ex Plus Medium, which was added on the apical side of 12 empty inserts (no cells) was kept inside the exposure chamber. After exposure, the cell culture medium was collected, stored in a sterile glass container, and used to characterize the ABS-emitted particles (mean hydrodynamic particle size and particle concentration) that would have reached and deposited on the surface of the epithelial layer using nanoparticle tracking analysis (NTA) (NanoSight NS300, Malvern Instruments, Worcestershire, UK), as previously described in detail.²² Note that when nanoscale particles deposit in culture medium, biomolecules

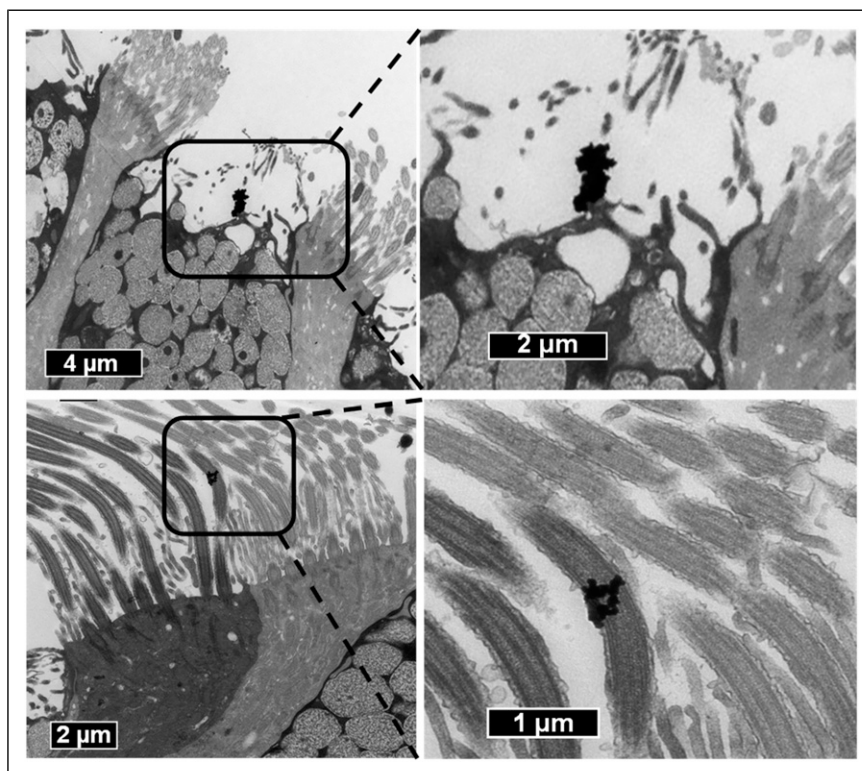


Figure 1. Representative TEM images of ABS agglomerated printer-emitted particles on the surface of NHBEs cells 24 h after exposure.

quickly attach to particle surfaces and can alter their biological activity and physical form compared with their native airborne state.⁴⁸ Given this rapid alteration of particle properties, as in our previous *in vitro* study, we only characterized particles in the culture medium as that was the form of the emissions that reached and deposited on the surface of the epithelial cell layer.²²

Particle mass ($\mu\text{g}/\text{cm}^2$) was calculated from the NTA data using a custom MATLAB script (MathWorks Inc. Natick, MA) as described previously.²⁴ Briefly, the mass distribution was calculated from the log-normal distribution curve generated from the NTA analysis with a bin (data point) every 0.5 nm, ranging from 0.5 to 600 nm, with the assumption that all particles were spherical and have a density of $1.04 \text{ g}/\text{cm}^3$ (density of ABS filament). Each data point in the count distribution was converted to mass using the following equation:

$$\text{Mass} = D \times (4/3) \times \pi \times r^3$$

Where: D = density, and r = radius of the particle. The mass from every bin in the distribution was then summed to calculate total particle mass. The assumption of spherical particle shape was approximately valid based on morphology of the individual particles that made up the agglomerates that deposited on the epithelial cell layer (see Figure 1).

For purposes of this study, measured particle number concentration and calculated particle mass were used to

express dose. The average particle number deposition of ABS-emitted particles was estimated by dividing the number of ABS particles per mL measured in the collection medium using NTA, to the surface area of the Transwell® inserts (1.12 cm^2). Similarly, for particle mass, the calculated value was divided per cell insert surface area (1.12 cm^2) to generate the average mass per insert. Further, to compare results to our previous *in vivo* study, the calculated particle mass value was normalized to the surface area of a rat lung by dividing by $4,000 \text{ cm}^2$, a typical approximate rat lung alveolar surface area.⁴⁹

Evaluation of Epithelial Barrier Integrity

As an important indicator of cell barrier integrity, TEER was measured using an Evom2 Epithelial Volt/ Ω meter equipped with 4 mm chopstick electrodes (World Precision Instruments Inc. Sarasota, FL). TEER was measured prior to the treatment and at defined time points of interest (0 and 24 hours after end of the exposure). To measure TEER, 0.5 mL of the corresponding fresh medium was added to the apical side of a 12-well insert, equilibrated for an additional 30 minute at 37°C , 5% CO_2 in air, and then the chopstick electrodes were placed on either side of the primary airway epithelium. All TEER values were measured in duplicate for each well and corrected for cell-free insert ($\approx 40 \Omega$) resistance and the surface area of a 12-well insert (1.12 cm^2).

Video Microscopy of Cilia Beating. The ciliary beating of live ALI tissue was visualized via phase-contrast microscopy before and after the treatment using a Revolve microscope (Echo Laboratories, San Diego, CA) at 40X magnification. The cilia movement was visualized prior to the treatment and at the end of the time points of interest (0 and 24 hours after end of the exposure).

Histology. Cultures were fixed in 10% neutral buffered formalin at room temperature until ready for processing. After fixation, the membrane inserts were rinsed twice with phosphate-buffered saline (PBS). The samples were dehydrated using a series of increasing ethanol concentrations, cleared with xylene, infiltrated with paraffin wax, and embedded in paraffin wax. Sections of 5 μ m thickness were cut using a Thermo Scientific™ HM 325 Rotary Microtome (Thermo Fisher Scientific, Waltham, MA). The sections were stained with Hematoxylin and Eosin (H&E) or Periodic acid–Schiff (PAS) using standard histological techniques and imaged using an Olympus BX63 light microscope and cellSens imaging software.

Transmission Electron Microscope Analysis. For TEM analysis, the cells on the Transwell® membrane were fixed with 2% paraformaldehyde/2.5% glutaraldehyde solution (Karnovsky's fixative) in sodium cacodylate buffer for at least 24 hours, subsequently washed three times with 8% sucrose/0.9% sodium chloride buffer and post-fixed with 1% osmium tetroxide (2 hours), washed with the sucrose/sodium chloride buffer, and stained *en bloc* with 1% tannic acid (1 hour) followed by 0.5% filtered uranyl acetate (1 hour). Afterwards, the cells were dehydrated in ascending ethanol series and embedded in Epon. From the embedded cells, ultrathin sections were cut parallel to the vertical axis of the inserts, mounted on copper grids and stained with 4% uranyl acetate. The sections were imaged on a JEOL JEM 1010 Transmission Electron Microscope (JEOL, Tokyo, Japan) operating at 80 kv with a side-mount digital AMT Orca camera system and software (autoVimation GmbH, Baden Württemberg, Germany).

Immunofluorescence Microscopy. Cultures on membranes were fixed in 4% (w/v) paraformaldehyde for 15 minute at room temperature. The samples were incubated in 0.5 mL permeabilization buffer (0.5% [v/v] Triton X-100 in Dulbecco's phosphate-buffered saline (D-PBS)) for 15 minutes, washed once with 0.5 mL D-PBS and blocked for 1 hour in 1% (w/v) bovine serum albumin (BSA) in D-PBS. Next, the cultures were incubated with primary antibodies diluted in blocking buffer for 1 hour at room temperature. The primary antibodies included rabbit anti-ZO-1 antibody (cat. 40-2200, Thermo Fisher Scientific Inc. Waltham, MA) used at a 1:100 dilution to identify tight junction formation, mouse anti-MUC5AC (45M1) antibody (cat. MA5-12178, Thermo Fisher Scientific Inc.) used at a 1:200 dilution to identify mucous cells, mouse anti-alpha tubulin antibody (B-5-1-2) (cat. 32-2500, Thermo

Fisher Scientific Inc.) used at a 1:200 dilution to identify cilia, and rabbit anti-e-cadherin (5HCLC) (cat. 710161, Thermo Fisher Scientific Inc.) used at a 1:200 dilution to identify adherent junction. The samples were subsequently washed three times with 0.5 mL D-PBS and incubated with secondary antibodies and 1 μ M Hoechst 33342 (cat. 62249, Thermo Fisher Scientific Inc.) for 1 hour at room temperature in the dark. The secondary antibodies included goat anti-mouse-Alexa Fluor 647 (cat. A-21236, Thermo Fisher Scientific Inc.) used at a 1:500 dilution and goat anti-rabbit Alexa Fluor 488 (cat. A-11008, Thermo Fisher Scientific Inc.) used at a 1:400 dilution. The samples were washed three times with 0.5 mL D-PBS, hold in 0.5 mL D-PBS until were visualized and imaged with a Revolve microscope (Echo Laboratories, San Diego, CA).

Cytotoxicity. Potential cytotoxic effects of ABS emissions were assessed by measuring cell viability and the release of the cytosolic enzyme lactate dehydrogenase (LDH) into the medium.

Cell Viability Assay. AlamarBlue™ Cell Viability Reagent (cat. DAL1025, Thermo Fisher Scientific), a non-toxic, cell-permeable compound, was used to assess cell viability. The assay was performed using medium collected from the apical compartment. After harvesting culture supernatants from the basolateral chamber for further analysis (LDH and cytokines analysis), 500 μ L of 10% AlamarBlue solution was added to each insert, and fresh medium was supplemented in the basolateral chamber. After 4 hour incubation at 37°C, the solution from the apical side of each insert was transferred in four wells (100 μ L per well) on a 96-well plate and fluorescence levels were quantified (ex/em 560/590 nm) using a Synergy H1 hybrid multi-mode microplate reader (BioTek Instruments, Inc, Winooski, VT). Three independent inserts ($n = 3$ inserts/treatment/time point) were conducted to obtain the mean and standard error for each treatment group (4 replicates of each sample-insert). Cell viability, proportional to the changes in fluorescence, was normalized to the controls and expressed as percentage viability.

Lactate Dehydrogenase Release Assay

The supernatant from the basal chamber was collected, and the release of the cytosolic enzyme LDH into the medium, indicative of cell membrane damage, was assayed spectrophotometrically by monitoring the reduction of nicotinamide adenine dinucleotide at 340 nm in the presence of lactate as per manufacturer instructions (Lactate Dehydrogenase Reagent Set, Pointe Scientific, Inc, Lincoln Park, MI). Three independent inserts ($n = 3$ inserts/treatment/time point) were conducted to obtain the mean and standard error for each treatment group (6 replicates of each sample-insert). LDH (U/L), defined as the amount of enzyme that catalyzes the transformation of 1 μ mol of substrate per minute, was normalized to the controls and expressed as percentage LDH (U/L).

Measurement of Cytokine Release. Media collected from the bottom (basolateral) wells was stored at -80°C until analysis. The concentrations of IL-17A, IL-21, IL-22, IL-23, IL-27, IL-31, MIP-3 α , IL-17A/F, IL-17B, IL-17D, IL-3, IL-9, GM-CSF, IL-23p40, IL-15, IL-16, IL-1 α , IL-5, IL-7, TNF- β , VEGF, IFN- γ , IL-10, IL-12p70, IL-13, IL-1 β , IL-2, IL-4, IL-6, IL-8, TNF- α , eotaxin, eotaxin-3, IP-10, MCP-1, MCP-4, MDC, MIP-1 α , MIP-1 β , and TARC (pg/mL) were measured using V-PLEX Human Biomarker Kits from Meso Scale Discovery (MSD, Meso Scale Discovery). Plates were read using MSD QuickPlex SQ 120 (Meso Scale Discovery) for electrochemiluminescence. Sample concentrations were derived from a standard curve plotted using a four-parameter logistic fit using MSD Workbench software ($N = 1\text{--}3$ inserts/treatment, $n = 2\text{--}3$ replicates each).

Statistics. All statistical analyses were performed in JMP v13 and RStudio Version 1.2.5001. Studies were performed in one independent experiments with $N = 1\text{--}3$ inserts/treatment, $n = 2\text{--}3$ replicates each. Assays measured below the limits of quantification were replaced with the lower limit of quantification as outlined by the manufacturer of V-PLEX Human Biomarker 54-Plex Kit. The TEER, viability, and LDH data are represented as mean \pm standard deviation. Two-way analysis of variance (treatment by time) was used to determine significant main and interaction effects. Residual Plots and Levene's test were used to assess the equality of variances while Normal Quantile Plots were used to assess the assumption of normality. Logarithmic transformations of the response proteins were used on proteins (MIP-3 α , GM-CSF, IL-6, MIP-1 β) that exhibited heterogeneous variance as shown by a funnel shaped Residual Plot. Significant results were further assessed with pooled t -tests to identify the specific main treatment effect and/or interaction effect. All analysis results were deemed statistically significant with a P -value of < 0.05 . Eight of the studied proteins, IL-17B, IL-3, IL-15, IL-1 α , IP-10, MCP-4, MIP-1 α , and TARC, exhibited non-normality and/or heterogeneous variance. To determine significant toxicity of these 8 proteins, a Kruskal Wallis Test was performed on treatment and time and post hoc comparisons were completed with the Mann-Whitney U Test.

Given the disproportionate effect outliers can have on the statistical results, outliers were identified using the interquartile range rule^{50,51} prior to statistical analysis. To begin, outliers were identified and removed from the raw data. Afterwards, the repetitions of each cytokine were averaged, and outliers of the clean dataset were identified.

Results

Particle Characterization and Deposition

The number-based size distribution of cell culture medium (background) and three samples of ABS 3-D printer-emitted

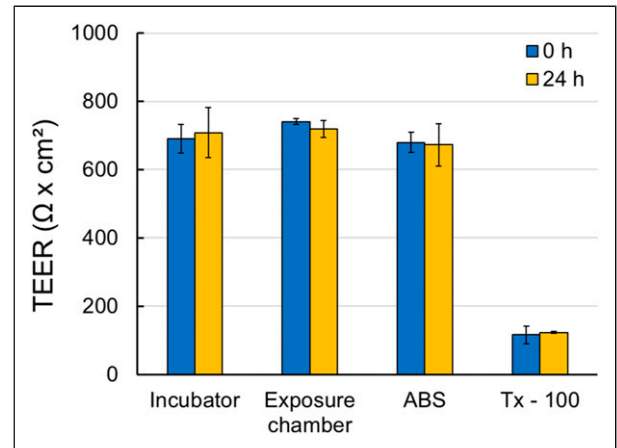


Figure 2. Barrier function of fully differentiated NHBEs measured by transepithelial electrical resistance (TEER). Values are means \pm standard deviation. $N = 2\text{--}5$ inserts, there were 2 replicates of each sample-insert. Tx-100 represents 0.2% Triton X-100.

particles collected in the cell culture medium were analyzed using NTA. The mean diameter of ABS particle in the medium varied from 150 to 198 nm (175 ± 24 nm), and the mode diameter varied from 136 to 165 nm (153 ± 15 nm). After background subtraction (plain cell culture medium), the average ABS particle concentration in medium was 8.73×10^7 particles/mL (standard deviation of 3.29×10^7), which is equivalent to 2.56×10^7 (standard deviation of 1.65×10^7) particles per insert (0.5 mL/insert, insert surface area 1.12 cm²), and corresponds to an average of 2.29×10^7 ABS particles per unit surface area of the ALI epithelium. Figure 1 shows the ABS printer-emitted particles agglomerated on the surface of NHBEs cells 24 hours after exposure. Based on a MATLAB calculation, the estimated average particle mass of ABS particle deposition per surface area of the epithelium was 0.144 ± 0.042 $\mu\text{g}/\text{cm}^2$.

Evaluation of NHBEs Epithelial Tight Junction Barrier Integrity

Disruption of barrier integrity enhances translocation of inhaled particles into the subepithelial space.⁵² To study junction function, permeability to small ions is measured by analyzing TEER. Before proceeding with the exposure (23 days post-ALI), the barrier integrity of the primary NHBEs was assessed and confirmed based on TEER measurements. Following 4 hour exposure to ABS emissions, no significant changes in TEER were observed between ABS-exposed cells and chamber-control cells or cells maintained in the incubator at the end time points, 0 or 24 hours post-treatment (Figure 2).

The integrity of the fully differentiated primary NHBEs was further confirmed by visualizing cilia movement which is essential for effective mucociliary clearance (Supplemental Video 1 Ciliary Beat). There were no noticeable differences between the treatments.

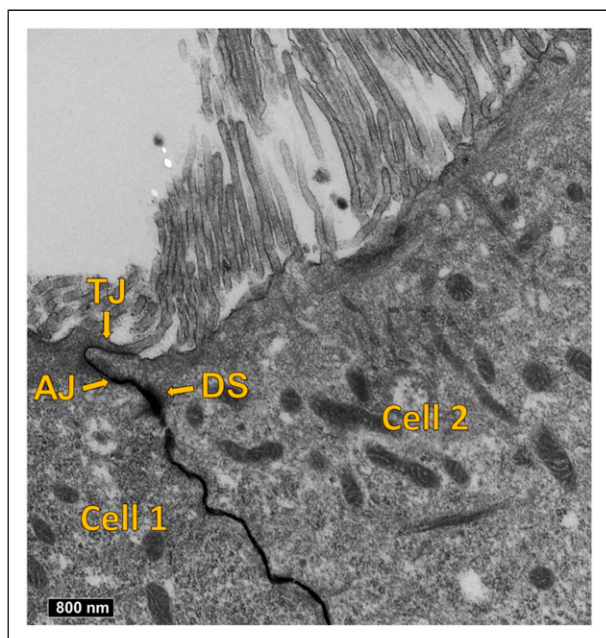


Figure 3. Representative TEM images of fully differentiated NHBEs showing junctional complex formation: tight-junctions (TJ), adherens junctions (AJ) and desmosomes (DS).

In addition, the junctional integrity of the fully differentiated primary NHBEs was assessed using TEM (Figure 3). In addition to tight junctions (TJ), adherens junctions (AJ) and desmosomes (DS) were identified, further confirming the presence of junctional complexes and barrier integrity within the NHBEs cultures. Tight-junction formation was also confirmed using immunofluorescence staining of the ZO-1 proteins (Figure 4). There were no noticeable differences between the treatments.

Overall, exposure of NHBEs to ABS emissions did not affect epithelium integrity at the conditions applied.

Evaluation of NHBEs Epithelium Differentiation

The bronchial epithelium was composed of fully differentiated airway epithelial cells (Figure 5), as noted from H&E and PAS staining. All of the major epithelial cell types, including mucous-secreting (goblet cells), and basal cells (b), and ciliated respiratory epithelial cells (c) were identified within the NHBEs layer. This was further confirmed by TEM imaging (Figure 6). Ciliated cells and mucous cells were present at the apical side of the epithelium. Histological analysis revealed that overall ciliation did not appear different between ABS-exposed cells and chamber-control cells or cells maintained in the incubator at the end time points, 0 or 24 hours post-treatment. Basement membrane and basal cells were present in NHBEs cultures stained with PAS and is seen as a distinct single thin layer at the interface between the epithelium and insert membrane.

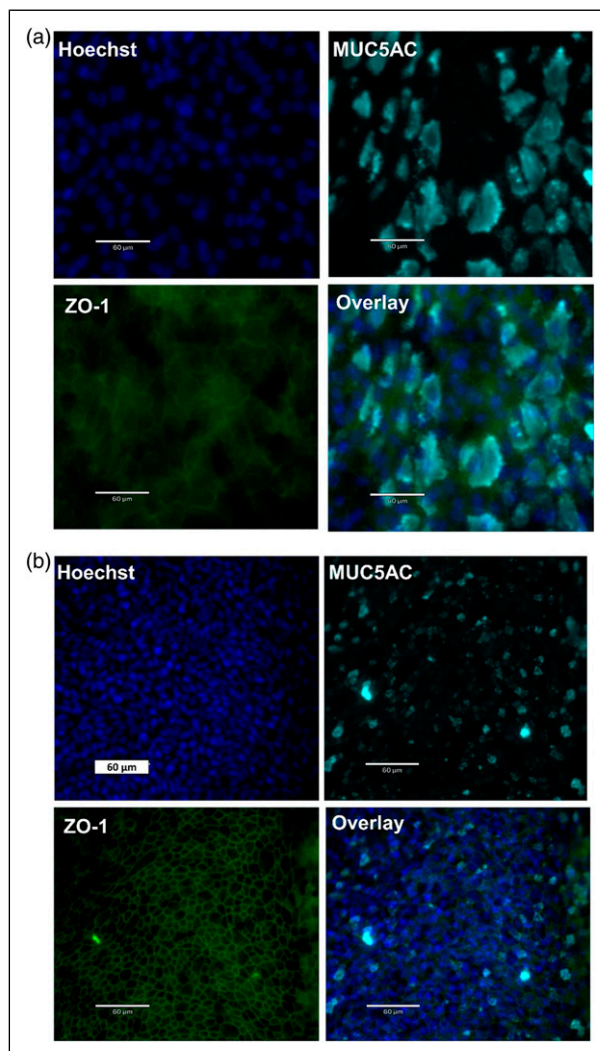


Figure 4. Representative labelled immunofluorescence images of fully differentiated NHBEs showing epithelial features, including MUC5AC-producing goblet cells (turquoise) and ZO-1 for tight junctions (green). Nuclei were stained with Hoechst 33342 (blue). (A) represents untreated cells and (B) represents ABS-treated cells.

The ultrastructure of the NHBEs' cilia configuration reveals both ciliary basal bodies, which are critical for cilia motility and sensory functions, and the 9 + 2 axoneme arrangements, microtubule-based cytoskeletal structure that forms the core of a cilium (Figure 7).

Immunofluorescence microscopy of the apical surface revealed the presence of mucous (goblet) and ciliated cells detected using the specific markers MUC5AC and α -tubulin, respectively (Figure 4 and Supplemental Figure 2 Immunofluorescence Images of Fully Differentiated NHBEs).

Overall, exposure of NHBEs to ABS emissions appeared to not affect ciliation or mucus production at the conditions applied.

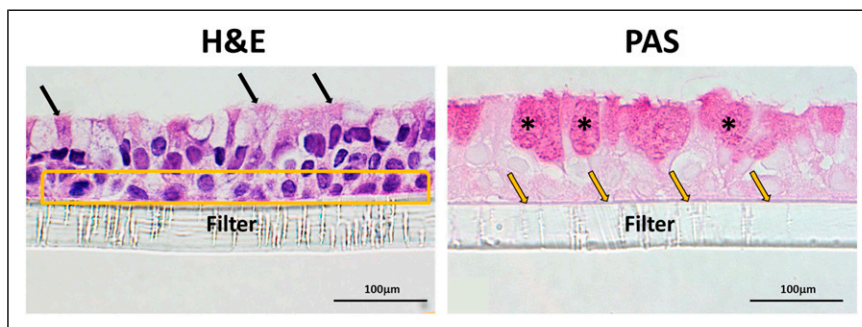


Figure 5. Representative photomicrographs of ALI epithelium before the exposure stained with hematoxylin and eosin (H&E) and Periodic acid–Schiff (PAS) stains showing normal architecture typical of the airway respiratory epithelium (40x magnification). Black arrows point to ciliated respiratory epithelial cells. The yellow box surrounds cells within the basal layer of the epithelium. Asterisks (*) highlight mucus containing goblet cells. Yellow arrows point to the basement membrane separating the epithelium from the underlying filter.

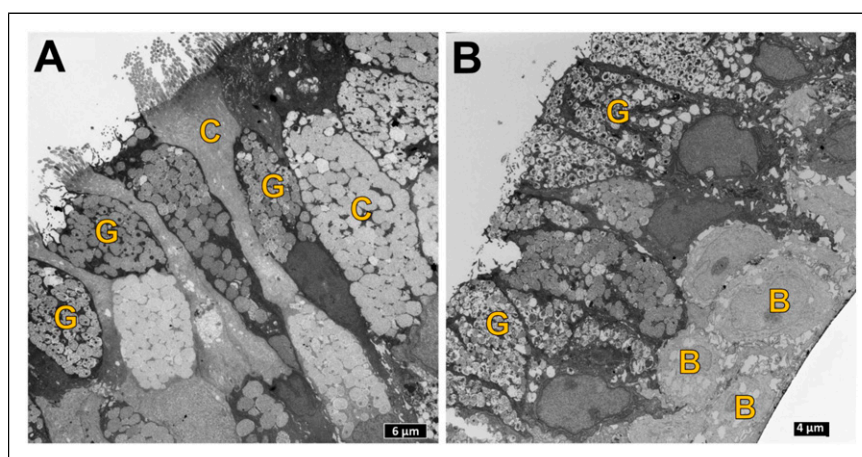


Figure 6. Representative TEM images showing the distribution of ciliated (C) and goblet (G) cells at the epithelial surface of fully differentiated NHBEs, and basal (B) cells at the basal region of the epithelium. (A) represent untreated cells and (B) represent ABS-treated cells.

Evaluation of Cytotoxic and Inflammatory Response in Differentiated NHBEs

The viability of cells exposed to ABS emissions was not statistically significant compared with incubator or exposure chamber controls (Figure 8A). Cytotoxicity was also evaluated by cell membrane integrity as indicated by LDH leakage from the exposed cells. Exposure to ABS emissions did not induce significant LDH release from the exposed cells compared to incubator or chamber controls (Figure 8B). No significant differences were observed between the 2 sets of untreated-control cells: inserts kept inside the emissions chamber covered, serving as exposure chamber negative controls (marked as “exposure chamber” samples) and inserts maintained in the incubator at normal growing conditions, serving as incubator controls (marked as “incubator” samples).

To investigate the inflammatory response from NHBEs cells exposed to ABS emissions, screening was performed for a panel of 43 cytokines and chemokines secreted into the

basolateral medium (Table 1). At the end of the exposure period (0 hour), statistically significant increased levels of IL-7 (1.65-fold) were seen in the cells exposed to ABS emissions compared to the cells maintained in the chamber control environment. At 24 hours after the exposure, significant increases in IL-17A (2.35-fold), VEGF (1.59-fold), IFN- γ (2.18-fold), IL-12p70 (1.78-fold), TNF- α (2.10-fold), and MIP-1 α (2.70-fold) were also noted in ABS-exposed cells compared to chamber control cells. No significant differences were observed between non-exposed chamber control cells and cells maintained in the incubator.

Discussion

In our previous studies, we evaluated the toxicity of FFF 3-D printer emissions using both *in vitro*²² and *in vivo* methods.²⁴ In the *in vitro* studies,²² human small airway epithelial cells (SAEC) were exposed to ABS 3-D printer emitted-particles freshly collected in the culture medium under submerged conditions. The *in vitro* studies established that exposure to

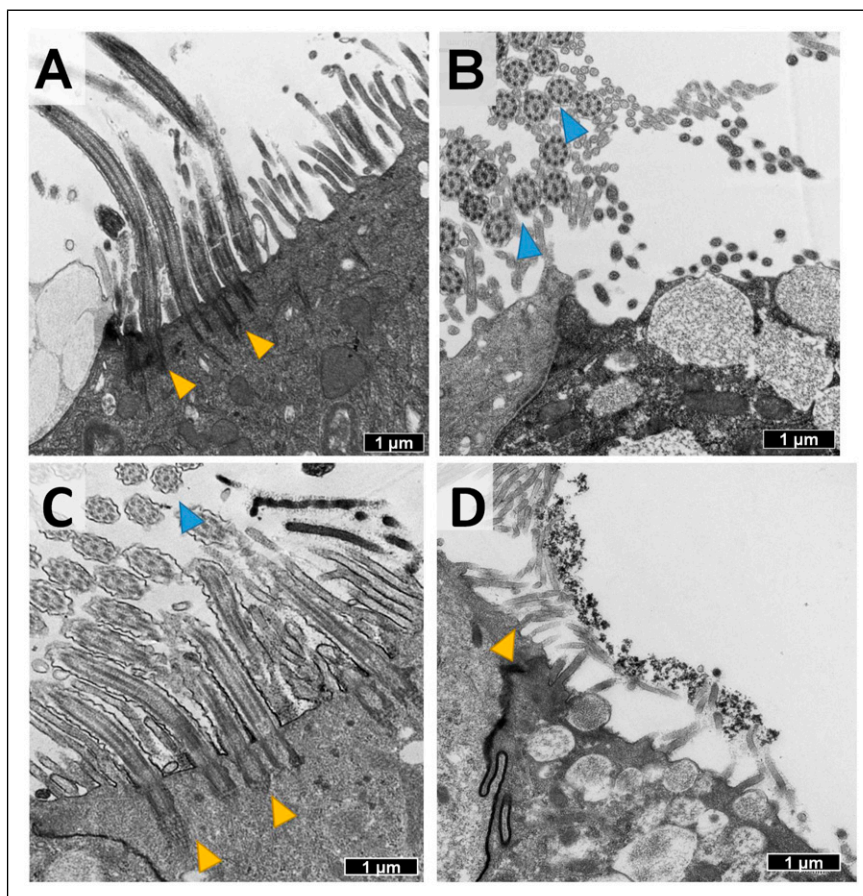


Figure 7. Representative TEM images of fully differentiated NHBs showing ultra-structural cilia formation in differentiated NHBs: (A) longitudinal sections of cilia and basal bodies (yellow arrowheads) and (B) transverse sections of cilia showing 9 + 2 axoneme arrangement (blue arrowheads). (A) and (B) represent untreated cells, and (C) and (D) represent ABS-treated cells. (D) also shows ABS agglomerated printer-emitted particles on the surface of NHBs cells 24 h after exposure.

ABS 3-D printer emissions collected in media induced dose-dependent cytotoxicity, oxidative stress, apoptosis, necrosis, and production of pro-inflammatory cytokines and chemokines in SAEC. In the *in vivo* studies,²⁴ male Sprague-Dawley rats were exposed to ABS emissions generated during real-time printing using a whole-body inhalation exposure system. The data of the *in vivo* studies demonstrated that a pro-inflammatory response was seen in bronchioalveolar lavage fluid (BALF) represented by an initial increase in IFN- γ and TNF- α Th1-type cytokines, followed by a switch to an anti-inflammatory response by day 15 of exposure, represented by a rise in the IL-10 Th2-type cytokine. Our *in vivo* studies showed that ABS 3-D emissions did not induce pulmonary oxidative stress responses nor histopathological changes in the lungs of rats at these exposure levels. It appears that there is a divergence between the results of our *in vitro* and *in vivo* studies. The *in vitro* studies demonstrated that exposure to ABS 3-D printer emissions induced toxicological changes in both cell signaling and cell structures, particularly the integrity of the cell membrane. However, in the *in vivo* studies at the concentration of 250 $\mu\text{g}/\text{cm}^3$ ³²⁴ demonstrated that ABS

emission exposure only induced inflammatory signaling changes in lungs with no significant pulmonary structural changes observed.

Considering the challenge of translating toxicological findings obtained in traditional submerged cell culture models or animal models to human context, in this study, we investigated the adverse effects of exposure to 3-D printer emissions using NHBs, a relevant human ALI organotypic airway tissue model. Results showed that the exposure of differentiated NHBs to ABS emissions in this ALI model did not affect epithelium integrity, ciliation, mucus production, or the induction of cytotoxicity, indicating no cellular structural changes. However, ABS emissions exposure induced the production of IFN- γ and TNF- α as well as significant increases in other cytokines/chemokines involved in the induction of Th1 responses and regulation of tight junction integrity. These ALI results reflect our *in vivo* studies²⁴ of increased levels of IFN- γ and TNF- α after ABS emissions exposure. Notably, the exposure conditions and settings utilized in the current ALI studies and *in vivo* studies²⁴ are similar, and both results indicate that the changes in cytokines/chemokines occur

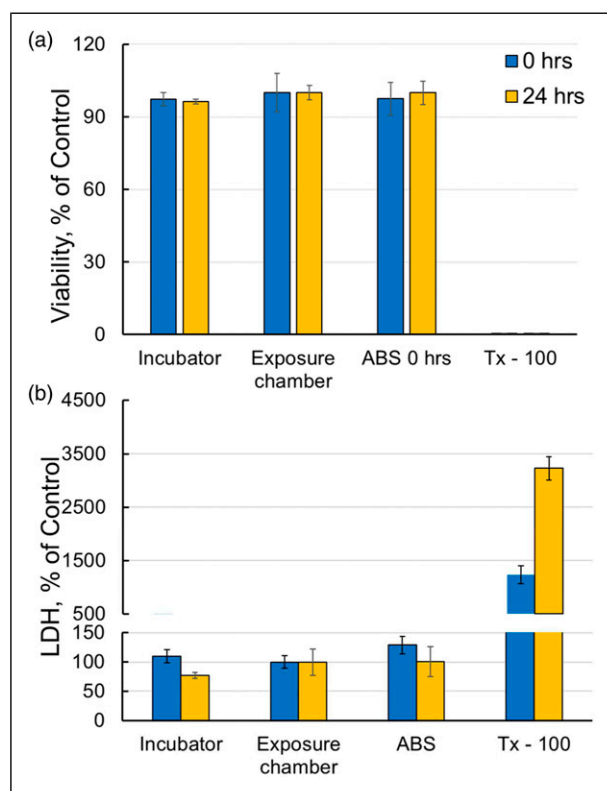


Figure 8. Cytotoxicity of fully differentiated NHBEs: cell viability (A) and LDH activity (B). Values represent % change in comparison to exposure chamber control. N = 3 inserts/treatment/time point, there were 4 replicates of each sample-insert. Tx-100 represents 0.2% Triton X-100.

without membrane damage or tissue morphological changes. Given that the exposure of the ALI *in vitro* model mimics the real-life scenario in the lung during particle inhalation, the findings of our current ALI studies could be more physiologically representative of the human-based 3-D printer emission exposure risk outcome than that observed in our previous submerged *in vitro* cell culture studies.²²

In the *in vitro* submerged culture studies, the particle concentration that was shown to cause a 10% decrease in viability and 20% increase of LDH²² has an estimated equivalent alveolar lung burden of ABS particles of 758 μg in rats.²⁴ Our *in vivo* studies,²⁴ estimated the day 30 alveolar deposition as 25.54 μg without the consideration of clearance and 12.10 μg with the clearance. These results indicated that the equivalent alveolar lung burden of the *in vitro* studies was approximately 30- to 60-times higher than that of the *in vivo* studies.²² In the current study, the estimated average particle mass of ABS emitted particle deposition per surface area of the NHBEs epithelium was $0.144 \pm 0.042 \mu\text{g}/\text{cm}^2$, which would result in an equivalent alveolar lung burden of ABS particles of $577 \pm 166 \mu\text{g}$ in the rat. Lung burden modeling indicate *in vitro* burden at ALI was 23- and 40-times higher than in the *in vivo* studies lung burden model without and with clearance,

respectively, and approximately 23% lower than in our *in vitro* SAEC studies.²² In this study the estimated particle mass deposited on the surface of the cells was calculated using several assumptions (particle shape, particle density, etc.), therefore this estimate of dosage could have errors. Accurately determining the dosage when conducting aerosol exposures with cells is a limitation to this type of exposure model.

Functional characteristics of airway epithelial cells, such as TEER across the epithelial layer,⁵³ ciliary motion,⁵⁴ and the formation of the junctional complex²⁶ are essential and key endpoints universally evaluated to study the potential adverse health effects of airborne toxicants or chemicals. Moreover, a change in any one of these parameters could be relevant to a variety of respiratory diseases.⁵⁵

A previous study⁵⁶ showed that ALI cultured airway epithelia from asthma patients display a decreased TEER in comparison to epithelia derived from healthy controls. In this study, the TEER values were lower, but not significantly, in ABS-exposed cells ($673\text{--}680 \Omega \times \text{cm}^2$) compared to chamber and incubator control cells ($691\text{--}741 \Omega \times \text{cm}^2$).

Abnormal ciliary function can lead to inadequate mucociliary clearance, which is associated with various respiratory diseases such as cystic fibrosis, and chronic obstructive pulmonary disease.⁵⁴ In the current study, light microscopy observation of beating cilia was visualized with a Revolve microscope. Rigorous observation of 2 entire inserts per treatment was performed, and vigorous beating of cilia in an apparently coordinated manner was noted as described in other ALI systems,^{57,58} demonstrating that the differentiated NHBEs have the potential for active mucociliary clearance. However, no noticeable differences were observed between the ABS-exposed cells and the chamber and incubator control cells.

The formation of junctional complexes (which include tight junctions, adherens junctions, and desmosomes) between neighboring epithelial cells creates an additional physical barrier against inhaled particulates, pathogens, and other xenobiotics from translocating into the interstitial compartment. The junctional-complex also forms a barrier against the movement of inflammatory mediators into the circulation, thereby limiting the activation and recruitment of immune cells to sites of injury.⁵⁹ Therefore, the evaluation of junctional-complex structures is an essential feature and important tool used in respiratory toxicity testing.

In the current study, the junctional complexes were observed and localized by immunofluorescence staining for E-cadherin and ZO-1, and also by TEM. To obtain a clear view of the ultrastructural arrangement, ALI cultures were sectioned, followed by TEM imaging. Tight junctions were seen at the apicolateral borders of epithelial cells in the differentiated NHBEs. In close proximity (ie, underneath) to tight junctions, are adherens junctions, emphasizing their interdependency, and the desmosome (localized more basally). Gasoline emissions is a heterogeneous mixture similar to 3-D printer emissions in regard to its physical state and composition.

Table 1. Cytokines Release Into Basolateral Cell Culture Media.

Marker (pg/mL ± SD)	0 h			24 h		
	Incubator	Chamber	ABS	Incubator	Chamber	ABS
IL-17A	5.24 ± 1.61	<2.25 [#]	3.76 ± 1.07*	3.00 ± 1.16	<2.25 [#]	3.85 ± 1.40*
IL-21	<1.65 [#]	<1.65 [#]	<1.65 [#]	<1.65 [#]	<1.65 [#]	<1.65 [#]
IL-22	<2.78 [#]	<2.78 [#]	<2.78 [#]	<2.78 [#]	<2.78 [#]	<2.78 [#]
IL-23	<3.18 [#]	<3.18 [#]	<3.18 [#]	<3.18 [#]	<3.18 [#]	<3.18 [#]
IL-27	63.07 ± 21.67	50.73 ± 8.63	56.82 ± 10.89	42.25 ± 12.86	32.79 ± 8.93	60.27 ± 25.16
IL-31	<4.22 [#]	<4.22 [#]	<4.22 [#]	<4.22 [#]	<4.22 [#]	<4.22 [#]
MIP-3α	1785.57 ± 1211.57	79.94 ± 11.79	176.78 ± 87.18	217.62 ± 286.53	48.78 ± 32.43	232.03 ± 251.60
IL-17A/F	<7.57 [#]	<7.57 [#]	<7.57 [#]	<7.57 [#]	<7.57 [#]	<7.57 [#]
IL-17B	<0.78 [#]	<0.78 [#]	<0.78 [#]	<0.87 [#]	1.22 ± 0.36	1.10 ± 0.32
IL-17D	<11.2 [#]	<11.2 [#]	<11.2 [#]	<11.2 [#]	<11.2 [#]	<11.2 [#]
IL-3	<8.84 [#]	<8.84 [#]	<8.84 [#]	<8.84 [#]	<8.84 [#]	<8.84 [#]
IL-9	41.20 ± 36.50	69.91 ± 21.34	55.33 ± 35.82	49.43 ± 29.46	46.60 ± 35.56	79.84 ± 51.20
GM-CSF	2.61 ± 1.52	4.21 ± 1.05	4.61 ± 3.27	15.23 ± 13.02	7.38 ± 0.82	16.45 ± 9.18
IL-23p40	<1.32 [#]	<1.32 [#]	<1.32 [#]	<1.32 [#]	<1.32 [#]	<1.32 [#]
IL-15	<0.54 [#]	<0.54 [#]	<0.54 [#]	0.93 ± 0.22	0.87 ± 0.06	1.24 ± 0.35*
IL-16	<19.1 [#]	<19.1 [#]	<19.1 [#]	<19.1 [#]	<19.1 [#]	<19.1 [#]
IL-1α	<2.01 [#]	6.28 ± 1.94	2.32 ± 0.57	2.33 ± 0.58	<2.01 [#]	2.87 ± 1.17
IL-5	<4.41 [#]	<4.41 [#]	<4.41 [#]	<4.41 [#]	<4.41 [#]	<4.41 [#]
IL-7	2.30 ± 1.17	1.91 ± 0.24	3.15 ± 0.60*	10.38 ± 3.02	10.90 ± 0.83	12.19 ± 0.88
TNF-β	<0.46 [#]	<0.46 [#]	<0.46 [#]	<0.46 [#]	<0.46 [#]	<0.46 [#]
VEGF	813.01 ± 617.13	517.89 ± 108.99	712.90 ± 274.62	1492.57 ± 261.22	1517.69 ± 67.07	2407.87 ± 679.24*
Eotaxin	<12.3 [#]	<12.3 [#]	<12.3 [#]	<12.3 [#]	<12.3 [#]	<12.3 [#]
Eotaxin-3	<7.14 [#]	<7.14 [#]	<7.14 [#]	<7.14 [#]	<7.14 [#]	<7.14 [#]
IFN-γ	5.31 ± 1.70	4.85 ± 1.00	7.03 ± 2.85	5.35 ± 3.37	4.04 ± 1.72	8.74 ± 2.54*
IL-10	2.41 ± 1.28	3.22 ± 0.58	3.84 ± 0.84	2.74 ± 1.06	2.69 ± 0.65	3.67 ± 0.91
IL-12p70	2.13 ± 0.90	2.26 ± 0.85	3.15 ± 1.11	1.94 ± 0.84	2.32 ± 0.55	4.44 ± 0.99*
IL-13	17.17 ± 9.87	20.87 ± 3.98	21.38 ± 8.28	13.68 ± 4.21	19.77 ± 5.03	29.71 ± 6.85*
IL-1β	3.02 ± 1.68	3.27 ± 0.40	4.04 ± 0.23	2.89 ± 0.98	2.88 ± 0.53	3.99 ± 0.92
IL-2	2.82 ± 1.60	3.04 ± 0.57	3.04 ± 1.42	2.78 ± 1.76	2.60 ± 0.71	3.71 ± 0.95
IL-4	0.86 ± 0.37	0.77 ± 0.16	0.93 ± 0.33	0.81 ± 0.59	0.71 ± 0.29	1.30 ± 0.27
IL-6	96.37 ± 117.01	9.09 ± 3.79	126.25 ± 120.36	88.14 ± 137.10	25.72 ± 10.85	265.24 ± 218.20
IL-8	1797.19 ± 51.93	1833.41 ± 28.82	1774.27 ± 50.31	1788.03 ± 64.34	1831.01 ± 70.99	1807.54 ± 67.22
TNF-α	6.58 ± 4.61	10.84 ± 3.08	11.05 ± 7.45	5.18 ± 2.50	8.84 ± 4.21	18.62 ± 7.94*
IP-10	27.16 ± 16.30	3.26 ± 0.18	16.00 ± 6.70	91.37 ± 38.89	85.41 ± 5.40	113.52 ± 61.24
MCP-1	18.71 ± 13.65	14.43 ± 2.46	22.37 ± 9.61	33.42 ± 9.36	25.50 ± 3.30	65.65 ± 30.69*
MCP-4	4.42 ± 1.80	<3.62 [#]	4.02 ± 0.84	4.34 ± 1.61	<3.62 [#]	6.64 ± 2.76
MDC	<88.3 [#]	<88.3 [#]	<88.3 [#]	<88.3 [#]	<88.3 [#]	<88.3 [#]
MIP-1α	14.41 ± 7.74	<9.69 [#]	11.18 ± 2.71	16.66 ± 9.38	<9.69 [#]	32.25 ± 15.49*
MIP-1β	4.99 ± 2.92	2.75 ± 1.14	4.22 ± 2.40	10.20 ± 2.40	8.00 ± 2.09	11.74 ± 4.91
TARC	3.42 ± 0.84	<2.34 [#]	2.43 ± 0.34	10.74 ± 3.78	10.79 ± 1.06	13.78 ± 3.73

Values represents mean ± standard deviation (SD). N = 2-5 inserts/treatment/time point; there were 3 replicates of each sample insert.

*P < 0.05 level different from the chamber control.

[#]indicates contains replicates that are below the lower limit of quantification.

Studies showed that exposure to gasoline engine emissions induced TEER reduction and LDH leakage in primary organotypic cultures of human bronchial epithelial cells.⁶⁰ However, in this 3-D printer emissions study, no noticeable differences were observed between the ABS-exposed cells and the chamber and incubator control cell at the conditions

applied, which could be explained by the lower delivered dose in our study compared to the gasoline studies.

The integrity of pseudostratified epithelium composed of ciliated and secretory cells and basal stem cells is vital for the process of mucociliary clearance by which multi-ciliated cells move mucus and trapped pathogens and particles out of the

lung.⁵⁴ Chronic exposure of primary HNBEs at the ALI to gasoline engine emissions impaired the cellular composition of the airway epithelium, increased the number of goblet cells.⁶⁰ In our 3-D printer emission study, the major cell types normally associated with *in vivo* airway epithelium (ie, ciliated, mucous or goblet, and basal cells) were present within the differentiated HNBEs cultures, and these were replicated in a pseudostratified morphology with ciliated cells interspersed with goblet cells facing the apical side and basal cells spreading along the basolateral membrane. Qualitative assessment of the epithelium did not indicate major degradation or de-differentiation changes between any of the treatments applied at any time point; there was no noticeable reduction in the number of ciliated cells, no increase in the number of epithelial vacuoles/gaps, and no adverse changes visible by H&E, PAS, and TEM. Ultrastructural analysis of ciliated cells by TEM demonstrated that cilia associated with differentiated HNBEs were of comparable morphology to those of *ex vivo* tissue, both in terms of the structure of the basal bodies and the 9 + 2 arrangement of axonemes. In the present study, evidence from PAS-stained histological sections and MUC5AC-labelled cultures demonstrated the presence of goblet cells and the production of mucus from differentiated HNBEs. The identification by TEM of mucus globules on the apical surface of HNBEs cultures and goblet cells actively extruding mucus confirmed these findings. Lastly, basal cells were identified from H&E-stained histological sections and TEM images. These cells represent an important component of airway epithelia because they function as progenitor (stem) cells which are involved in repair and regeneration following injury.⁶¹

The measurement of cytotoxicity is an important biomarker in the evaluation of toxicants. In the current study, the applied treatments (except for the positive control) had no effect on cellular viability. The LDH release into the media was not statistically significant in the ABS exposed cells. However, significant increases in IL-12p70, IFN- γ , TNF- α , VEGF, IL-17A, and MIP-1 α were observed. Similar findings have been reported with other respiratory toxicants;^{62,63} these studies determined that functional changes and oxidative metabolism occurs at concentrations (4×10^3 – 4×10^7 glass fibers/ml) that do not significantly affect the integrity of the cellular membrane and that the cellular function is typically affected before membrane damage, and we speculate that the cytokines responses may be a more sensitive measure of cytotoxic effects. Similarly, in our *in vivo* studies,²⁴ cytokine changes occurred before structural changes.

The ability of NPs to induce persistent inflammation in tissues is a key factor in determining their toxicity and also a fundamental mechanistic paradigm in nanotoxicology.^{64,65} Although the exposure of differentiated HNBEs to ABS emissions did not affect epithelium integrity, ciliation, mucus production, or induced cytotoxicity, a significant increase in cytokines involved in the induction of Th1 responses and regulation of tight junction integrity was observed. Similarly, after 3-D printer emissions exposure, in both *in vivo*²⁴ and

*in vitro*²² inflammation was the most sensitive biological response parameter measured in these studies.

In our previous *in vivo* study,²⁴ IFN- γ and IL-10 were significantly increased in the BALF of rats after ABS emission exposure of 1 and 4 days. In the ALI study, IL-7, IL-13, IL-15, IL-12p70, IFN- γ , TNF- α , VEGF, IL-17A, MCP-1, and MIP-1 α cytokines were significantly increased in differentiated HNBEs. There was no consistent and demonstrative overlap between the cytokines detected and measured in our three studies. First, this may reflect that the time-dependent release of cytokines was not captured in the time endpoints selected for this ALI study. Second, additional studies using multiple concentrations are needed to establish an exposure dose-response relationship; third, this could reflect species differences (rat and human); fourth, differences in the cell types used in *in vitro* studies; and fifth, in the rat and ALI, the exposures were to the gas phase and the particle-phase emissions, whereas the submerged *in vitro* the exposure was to particles and gases trapped in the culture media during collection, with the latter, we could have lost important gases or had lower concentrations of gases compared with the ALI and *in vivo* set-ups.

In our first *in vitro* study,²² IL-16 increased at the highest level compared to the other measured cytokines in human small airway epithelial cells (SAEC) at 24 hours post-exposure of ABS emissions in suspension. IL-16 is a mediator of inflammation by promoting the secretion of other pro-inflammatory cytokines (IL-1 β , IL-6, and TNF- α).⁶⁶ IL-16 plays a key role in asthma,⁶⁷ in particular with airway hyper-responsiveness and up-regulation of IgE antibodies.⁶⁸ Another cytokine recently found to be involved in severe asthma pathogenesis is IL-17A.⁶⁹ In the current ALI study, IL-17A was increased in the differentiated HNBEs exposed to ABS emissions, suggesting that ABS emissions might be exacerbating asthma pathogenesis.

IL-12p70 and TNF- α were significantly increased in both *in vitro* studies. TNF- α was also slightly increased in BALF in the *in vivo* study at day 1 of exposure. IL-12p70 is a pro-inflammatory cytokine which promotes induction of Th1 (IFN- γ , TNF- α) and cytotoxic T cell responses.⁷⁰ Similarly, in this study, increased levels of IL-12p70 was concomitant with increases in IFN- γ and TNF- α , which are well-known for their role in the regulation of tight junction integrity.⁷¹ TNF- α is involved in acute systemic inflammation, regulation of tight junction integrity⁷⁰ and expression and secretion of MUC5AC.⁷² TNF- α decreases the protein expression of the tight junction proteins claudin-1, occludin, and ZO-1, as well as induces cytoskeletal F-actin rearrangement and the mislocalization of occludin and ZO-1.^{73,74} In this study, quantification of ZO-1 and MUC5AC following exposure to ABS emissions was not possible; therefore, future studies can elucidate if a relationship occurs from 3-D printer emission exposures.

IFN- γ , similar to TNF- α , disrupts the barrier integrity of epithelial and endothelial cells both *in vivo*⁷⁵ and *in vitro*^{76–80}

IFN- γ induces an increase in barrier permeability through the reduction of ZO-1 and occludin expression in an adenosine monophosphate-activated protein kinase (AMPK)-dependent pathway.⁸¹ Ng et al⁷⁸ suggests that p38 MAP kinase is activated in response to IFN- γ and causes actin rearrangement and altered cell morphology, which in turn mediates endothelial cell hyperpermeability. IFN- γ was found significantly increased in this ALI study and in our *in vivo* study. Disruption of epithelial barrier function triggered by the elevated IFN- γ is accompanied by reduced expression of the TJ proteins, zonula occludens ZO-1 and occludin.^{76,80}

The simultaneous presence of both TNF- α and IFN- γ cytokines suggests that exposure to ABS emissions might have a detrimental effect on epithelium barrier integrity through the disassociation of tight junction proteins.⁸² In this study, TEER was not statistically significant between any of the groups.

TNF- α and VEGF have been reported to be involved in the expression and secretion of MUC5AC,⁷² a major mucin glycoprotein hypersecreted in asthmatic individuals.^{83,84} VEGF is also a potent stimulator of inflammation, as well as airway and vascular remodeling.⁸⁵ MCP-1 α was slightly increased in ALI exposed cells. The elevations of IL-17A, MIP-1 α , and MCP-1 α following exposure to ABS emissions could promote generation of other pro-inflammatory cytokines and chemokines, which might lead to the migration and infiltration of neutrophils and monocytes/macrophages to the inflammation site, as has been previously reported.⁸⁶⁻⁸⁸ In addition, IL-17A can synergize with other proinflammatory cytokines such as TNF- α and IFN- γ ,⁸⁹ which were found to be increased in our exposure model as well.

The dysregulation of pro- and anti-inflammatory cytokines and chemokines is a central aspect in the promotion of inflammation.^{90,91} However, the distinction between pro- and anti-inflammatory effects is not entirely clear mainly due to pathway interactions and their dual pro- and anti-inflammatory effects.⁹⁰ Therefore, it is often difficult to use cytokines levels as a diagnostic tool.

There are several commercially available exposure systems⁹²⁻⁹⁹ largely used in the field of *in vitro* inhalation toxicology to test a variety of airborne substances, such as nanoparticles, gases, and complex mixtures. These air-liquid interface cell exposure systems¹⁰⁰⁻¹⁰⁴ have been used for aerosolization of NP-containing liquid aerosols. The deposition rates are known to vary among these exposure systems. From the total aerosolized amount in nebulizers, reported particle deposition ranged between 0.037% for aerosolized polystyrene particles/well in one system,¹⁰⁴ 0.157% in the other system,¹⁰³ and 2.8% in the optimized exposure system.¹⁰⁵ Indeed, it has been found that in these systems, the deposition is particle-dependent.¹⁰⁴ We attempted to utilize one of these systems in our studies; however, due to the difficulty of delivering a reliable dose, we instead used the exposure chamber developed for our animal exposure studies.²⁴ Therefore, both our previous *in vivo* studies and the current *in vitro* studies used the same exposure chamber.

Some advantages regarding the exposure method employed in this study are that: (1) the cells were exposed to aerosols and gases via “dry” dispersion (i.e., not previously collected in liquid prior to dosing cells), which is comparable to the realistic exposure scenarios of the proximal airway experienced by humans including cell-chemical interactions, and faster uptake kinetics of the test material;¹⁰⁶ and (2) the cells were exposed to emissions freshly generated during real-time 3-D printing avoiding the “ageing” effect of long-term storage of NPs as has been previously reported.¹⁰⁷ With regard to the toxicological effects, overall, the biological effects noted here resulted from the exposure to the complex mixture composed of ultrafine particles and volatile organic compounds.

This current acute ALI exposure study presented here is phase one of our 3-D printer emissions studies. Results obtained from this phase study showed that the currently used ALI-based exposure chamber is promising for testing the respiratory toxicity of 3-D printer emissions. To develop a more sophisticated ALI exposure chamber system, some structural changes are needed to include more sample ports, optimized and validated to ensure a uniform particle deposition throughout the chamber.

Conclusions

At the current experimental conditions, exposure of differentiated NHBES to ABS emissions does not affect epithelium integrity, ciliation, and mucus production, nor induce cytotoxicity. However, after 4 hours exposure to ABS emissions, we observed increased IL-7 secretion, and at 24 hours after exposure, IL-17A, VEGF, IFN- γ , IL-12p70, TNF- α , and MIP-1 α compared to chamber control cells, which correlates with the findings from our previous *in vivo* studies in rats. In conclusion, both our *in vivo* and the ALI-based *in vitro* studies indicate that the FFF 3-D printer emissions could induce minimal toxicological effects. This study is significant as it is the first study to evaluate the pulmonary toxicity of 3-D printer emissions using an advanced human ALI organotypic airway tissue model derived from primary normal bronchial epithelial cells and compared current findings to previously published *in vivo* results, indicating that ALI-based model could be a promising one to predict 3-D printer emissions-induced toxicity *in vitro*.

Author Contributions

Farcas, M. T. contributed to conception and design, contributed to acquisition, analysis, and interpretation, drafted manuscript, and critically revised manuscript; McKinney, W. contributed to conception and design, contributed to acquisition, analysis, and interpretation, drafted manuscript, and critically revised manuscript; Coyle, J. contributed to conception, contributed to acquisition, drafted manuscript, and critically revised manuscript; Orandle, M. contributed to conception, contributed to acquisition, analysis, and interpretation, drafted manuscript, and critically revised manuscript; Kyle Mandler, W. contributed to conception, contributed to

acquisition, drafted manuscript, and critically revised manuscript; Stefaniak, A. B. contributed to conception and design, contributed to acquisition, analysis, and interpretation, drafted manuscript, and critically revised manuscript; Bowers, L. contributed to conception, contributed to acquisition, and critically revised manuscript; Battelli, L. contributed to acquisition and critically revised manuscript; Richardson, D. contributed to acquisition and critically revised manuscript; Hammer, M. A. contributed to conception, contributed to acquisition, and critically revised manuscript; Friend, S. A. contributed to acquisition and critically revised manuscript; Service, S. contributed to design, contributed to acquisition, analysis, and interpretation, drafted manuscript, and critically revised manuscript; Kashon, M. contributed to design, contributed to acquisition, analysis, and interpretation, drafted manuscript, and critically revised manuscript; Qi, C. contributed to design, contributed to acquisition, analysis, and interpretation, drafted manuscript, and critically revised manuscript; Hammond, D. R. contributed to design, contributed to acquisition, analysis, and interpretation, drafted manuscript, and critically revised manuscript; Thomas, T. A. contributed to design and critically revised manuscript; Matheson, J. contributed to design and critically revised manuscript; Qian Y. contributed to conception and design, contributed to acquisition, analysis, and interpretation, drafted manuscript, and critically revised manuscript. All authors gave final approval and agree to be accountable for all aspects of work ensuring integrity and accuracy.

Declaration of Conflicting Interests

The author(s) declared no potential conflicts of interest with respect to the research, authorship, and/or publication of this article.

Funding

The author(s) disclosed receipt of the following financial support for the research, authorship, and/or publication of this article: This investigation was supported by U.S. Consumer Product Safety Commission (CPSC) and the National Institute for Occupational Safety and Health (NIOSH), Project [093909NF].

Disclaimer

The findings and conclusions in this report are those of the authors and do not necessarily represent the official position of the National Institute for Occupational Safety and Health (NIOSH), Centers for Disease Control and Prevention (CDC). Mention of any company or product does not constitute endorsement by NIOSH/CDC. This work has not been reviewed or approved by and does not necessarily represent the views of the Commission.

ORCID iD

Yong Qian  <https://orcid.org/0000-0001-7138-0141>

Supplemental material

Supplemental material for this article is available online.

References

1. Ding S, Ng BF, Shang X, Liu H, Lu X, Wan MP. The characteristics and formation mechanisms of emissions from thermal

- decomposition of 3D printer polymer filaments. *Sci Total Environ.* 2019;692:984-994.
2. Gu J, Wensing M, Uhde E, Salthammer T. Characterization of particulate and gaseous pollutants emitted during operation of a desktop 3D printer. *Environ Int.* 2019;123:476-485.
3. Katz EF, Goetz JD, Wang C, et al. Chemical and physical characterization of 3D printer aerosol emissions with and without a filter attachment. *Environ Sci Technol.* 2020;54(2):947-954.
4. Kwon O, Yoon C, Ham S, et al. Characterization and control of nanoparticle emission during 3D printing. *Environ Sci Technol.* 2017;51(18):10357-10368.
5. Potter PM, Al-Abed SR, Lay D, Lomnicki SM. VOC emissions and formation mechanisms from carbon nanotube composites during 3D printing. *Environ Sci Technol.* 2019;53(8):4364-4370.
6. Stabile L, Scungio M, Buonanno G, Arpino F, Ficco G. Airborne particle emission of a commercial 3D printer: the effect of filament material and printing temperature. *Indoor Air.* 2017;27(2):398-408.
7. Steinle P. Characterization of emissions from a desktop 3D printer and indoor air measurements in office settings. *J Occup Environ Hyg.* 2016;13(2):121-132.
8. Vance ME, Pegues V, Van Montfrans S, Leng W, Marr LC. Aerosol emissions from fuse-deposition modeling 3D printers in a chamber and in real indoor environments. *Environ Sci Technol.* 2017;51(17):9516-9523.
9. Yi J, LeBouf RF, Duling MG, et al. Emission of particulate matter from a desktop three-dimensional (3D) printer. *J Toxicol Environ Health.* 2016;79(11):453-465.
10. Azimi P, Zhao D, Pouzet C, Crain NE, Stephens B. Emissions of ultrafine particles and volatile organic compounds from commercially available desktop three-dimensional printers with multiple filaments. *Environ Sci Technol.* 2016;50(3):1260-1268.
11. Deng Y, Cao S-J, Chen A, Guo Y. The impact of manufacturing parameters on submicron particle emissions from a desktop 3D printer in the perspective of emission reduction. *Build Environ.* 2016;104:311-319.
12. Floyd EL, Wang J, Regens JL. Fume emissions from a low-cost 3-D printer with various filaments. *J Occup Environ Hyg.* 2017;14(7):523-533.
13. Mendes L, Kangas A, Kukko K, et al. Characterization of emissions from a desktop 3D printer. *J Ind Ecol.* 2017;21(S1):S94-S106.
14. Zhang Q, Wong JPS, Davis AY, Black MS, Weber RJ. Characterization of particle emissions from consumer fused deposition modeling 3D printers. *Aerosol Sci Technol.* 2017;51(11):1275-1286.
15. Zhou Y, Kong X, Chen A, Cao S. Investigation of ultrane particle emissions of desktop 3D printers in the clean room. *Procedia Eng.* 2015;121:506-512.
16. Bharti N, Singh S. Three-dimensional (3D) printers in libraries: Perspective and preliminary safety analysis. *J Chem Educ.* 2017;94(7):879-885.

17. Stephens B, Azimi P, El Orch Z, Ramos T. Ultrafine particle emissions from desktop 3D printers. *Atmos Environ*. 2013;79:334-339.
18. Wojtyla S, Klama P, Baran T. Is 3D printing safe? Analysis of the thermal treatment of thermoplastics: ABS, PLA, PET, and nylon. *J Occup Environ Hyg*. 2017;14(6):D80-D85.
19. Yi J, Duling MG, Bowers LN, et al. Particle and organic vapor emissions from children's 3-D pen and 3-D printer toys. *Inhal Toxicol*. 2019;31(13-14):432-445.
20. Youn J-S, Seo J-W, Han S, Jeon K-J. Characteristics of nanoparticle formation and hazardous air pollutants emitted by 3D printer operations: From emission to inhalation. *RSC Adv*. 2019;9(34):19606-19612.
21. Zhang Q, Pardo M, Rudich Y, et al. Chemical composition and toxicity of particles emitted from a consumer-level 3D printer using various materials. *Environ Sci Technol*. 2019;53(20):12054-12061.
22. Farcas MT, Stefaniak AB, Knepp AK, et al. Acrylonitrile butadiene styrene (ABS) and polycarbonate (PC) filaments three-dimensional (3-D) printer emissions-induced cell toxicity. *Toxicol Lett*. 2019;317:1-12.
23. Stefaniak AB, LeBouf RF, Duling MG, et al. Inhalation exposure to three-dimensional printer emissions stimulates acute hypertension and microvascular dysfunction. *Toxicol Appl Pharmacol*. 2017;15335:1-5.
24. Farcas MT, McKinney W, Qi C, et al. Pulmonary and systemic toxicity in rats following inhalation exposure of 3-D printer emissions from acrylonitrile butadiene styrene (ABS) filament. *Inhal Toxicol*. 2020;32(11-12):403-418.
25. Cidem A, Bradbury P, Traini D, Ong HX. Modifying and Integrating in vitro and ex vivo respiratory models for inhalation drug screening. Review. *Front Bioeng Biotechnol*. 2020;8:1256.
26. Upadhyay S, Palmberg L. Air-liquid interface: relevant in vitro models for investigating air pollutant-induced pulmonary toxicity. *Toxicol Sci*. 2018;164(1):21-30.
27. Prytherch Z, Bérubé K. Cellular in vitro testing: methods and protocols. In: Haycock J, Ahluwalia A, Wilkinson MJ, eds. *Advances in In-Vitro 3D Lung Cell Culture*. Singapore: Pan Stanford Publishing; 2014.
28. Parent RA. *Comparative Biology of the Normal Lung*. Damariscotta, Maine: Academic Press; 2015.
29. Bogdanffy MS, Keller DA. Metabolism of xenobiotics by the respiratory tract. *Toxicology of the Lung*. 1999;3:383-407.
30. Sarangapani R, Clewell HJ, Cruzan G, Andersen ME. Comparing respiratory-tract and hepatic exposure-dose relationships for metabolized inhaled vapors: A pharmacokinetic analysis. *Inhal Toxicol*. 2002;14(8):835-854.
31. Hofmann W, Koblinger L, Martonen T. Structural differences between human and rat lungs: Implications for Monte Carlo modeling of aerosol deposition. *Health Phys*. 1989;57:41-46.
32. Miller F, Mercer R, Crapo J. Lower respiratory tract structure of laboratory animals and humans: Dosimetry implications. *Aerosol Sci Technol*. 1993;18(3):257-271.
33. Morfeld P, Bruch J, Levy L, et al. Translational toxicology in setting occupational exposure limits for dusts and hazard classification - a critical evaluation of a recent approach to translate dust overload findings from rats to humans. *Part Fibre Toxicol*. 2015;12:3-3.
34. Seok J, Warren HS, Cuenca AG, et al. Genomic responses in mouse models poorly mimic human inflammatory diseases. *Proc Natl Acad Sci USA*. 2013;110(9):3507-3512.
35. Lacroix G, Koch W, Ritter D, et al. Air-liquid Interface in vitro models for respiratory toxicology research: Consensus workshop and recommendations. *Appl In Vitro Toxicol*. 2018;4(2):91-106.
36. Clippinger AJ, Allen D, Jarabek AM, et al. Alternative approaches for acute inhalation toxicity testing to address global regulatory and non-regulatory data requirements: An international workshop report. *Toxicol In Vitro*. 2018;48:53-70.
37. Faber SC, McCullough SD. Through the looking glass: In vitro models for inhalation toxicology and interindividual variability in the airway. *Appl In Vitro Toxicol*. 2018;4(2):115-128.
38. Dvorak A, Tilley AE, Shaykhiev R, Wang R, Crystal RG. Do airway epithelium air-liquid cultures represent the in vivo airway epithelium transcriptome? *Am J Respir Cell Mol Biol*. 2011;44(4):465-473.
39. Thaikoottathil JV, Martin RJ, Zdunek J, Weinberger A, Rino JG, Chu HW. Cigarette smoke extract reduces VEGF in primary human airway epithelial cells. *Eur Respir J*. 2009;33(4):835-843.
40. Zarcone MC, Duistermaat E, van Schadewijk A, Jedynska A, Hiemstra PS, Kooter IM. Cellular response of mucociliary differentiated primary bronchial epithelial cells to diesel exhaust. *Am J Physiol Lung Cell Mol Physiol*. 2016;311(1):L111-L123.
41. Amatngalim GD, van Wijck Y, de Mooij-Eijk Y, et al. Basal cells contribute to innate immunity of the airway epithelium through production of the antimicrobial protein RNase 7. *J Immunol*. 2015;194(7):3340-3350.
42. Palermo LM, Porotto M, Yokoyama CC, et al. Human para-influenza virus infection of the airway epithelium: Viral hemagglutinin-neuraminidase regulates fusion protein activation and modulates infectivity. *J Virol*. 2009;83(13):6900-6908.
43. Kesimer M, Kirkham S, Pickles RJ, et al. Tracheobronchial air-liquid interface cell culture: A model for innate mucosal defense of the upper airways? *Am J Physiol Lung Cell Mol Physiol*. 2009;296(1):L92-L100.
44. Movia D, Bruni-Favier S, Prina-Mello A. In vitro alternatives to acute inhalation toxicity studies in animal models—a perspective. Perspective. *Front Bioeng Biotechnol*. 2020;8:549.
45. Stefaniak AB, LeBouf RF, Yi J, et al. Characterization of chemical contaminants generated by a desktop fused deposition modeling 3-dimensional printer. *J Occup Environ Hyg*. 2017;14(7):540-550.
46. Davis AY, Zhang Q, Wong JPS, Weber RJ, Black MS. Characterization of volatile organic compound emissions from consumer level material extrusion 3D printers. *Build Environ*. 2019;160:106209.
47. Vidakis N, Petousis M, Maniadi A, Koudoumas E, Vairis A, Kechagias J. Sustainable additive manufacturing: Mechanical

- response of acrylonitrile-butadiene-styrene over multiple recycling processes. *Sustainability*. 2020;12(9):3568.
48. Kendall M, Hodges NJ, Whitwell H, Tyrrell J, Cangul H. Nanoparticle growth and surface chemistry changes in cell-conditioned culture medium. *Philos Trans R Soc Lond B Biol Sci*. 2015;370(1661):20140100-20140100.
 49. Oller AR, Oberdörster G. Incorporation of particle size differences between animal studies and human workplace aerosols for deriving exposure limit values. *Regul Toxicol Pharmacol*. 2010;57(2-3):181-194.
 50. Faraway JJ. *Linear Models with R*. vol 2. Boca Raton, Florida: Chapman & Hall/CRC; 2015.
 51. Faraway JJ. *Extending the Linear Model with R*. Boca Raton, Florida: CRC Press; 2016.
 52. Rezaee F, Georas SN. Breaking barriers. New insights into airway epithelial barrier function in health and disease. *Am J Respir Cell Mol Biol*. 2014;50(5):857-869.
 53. Srinivasan B, Kolli AR, Esch MB, Abaci HE, Shuler ML, Hickman JJ. TEER measurement techniques for in vitro barrier model systems. *J Lab Autom*. 2015;20(2):107-126.
 54. Seybold ZV, Mariassy AT, Stroh D, Kim CS, Gazeroglu H, Wanner A. Mucociliary interaction in vitro: Effects of physiological and inflammatory stimuli. *J Appl Physiol*. 1990;68(4):1421-1426.
 55. Cao X, Coyle JP, Xiong R, et al. Invited review: Human air-liquid-interface organotypic airway tissue models derived from primary tracheobronchial epithelial cells—overview and perspectives. *In Vitro Cell Dev Biol Animal*. 2020;57(2):104-132.
 56. Xiao C, Puddicombe SM, Field S, et al. Defective epithelial barrier function in asthma. *J Allergy Clin Immunol*. 2011;128(3):549-556.
 57. Sears PR, Davis CW, Chua M, Sheehan JK. Mucociliary interactions and mucus dynamics in ciliated human bronchial epithelial cell cultures. *Am J Physiol Lung Cell Mol Physiol*. 2011;301(2):L181-L186.
 58. Munkholm M, Mortensen J. Mucociliary clearance: Pathophysiological aspects. *Clin Physiol Funct Imag*. 2014;34(3):171-177.
 59. Rezaee F, Georas SN. Breaking barriers. New insights into airway epithelial barrier function in health and disease. *Am J Respir Cell Mol Biol*. 2014;50(5):857-869.
 60. Cervena T, Vojtisek-Lom M, Vrbova K, et al. Ordinary gasoline emissions induce a toxic response in bronchial cells grown at air-liquid interface. *Int J Mol Sci*. 2021;22(1):79.
 61. Rock JR, Randell SH, Hogan BLM. Airway basal stem cells: A perspective on their roles in epithelial homeostasis and remodeling. *Disease Models Mechanisms*. 2010;3(910):545.
 62. Castranova V, Bowman L, Reasor MJ, Miles PR. Effects of heavy metal ions on selected oxidative metabolic processes in rat alveolar macrophages. *Toxicol Appl Pharmacol*. 1980;53(1):14-23.
 63. Zeidler-Erdely PC, Calhoun WJ, Ameredes BT, et al. In vitro cytotoxicity of manville code 100 glass fibers: Effect of fiber length on human alveolar macrophages. *Part Fibre Toxicol*. 2006;3(1):5.
 64. Øvrevik J, Refsnes M, Låg M, Holme JA, Schwarze PE. Activation of proinflammatory responses in cells of the airway mucosa by particulate matter: Oxidant- and non-oxidant-mediated triggering mechanisms. *Biomolecules*. 2015;5(3):1399-1440.
 65. Nho R. Pathological effects of nano-sized particles on the respiratory system. *Nanomedicine*. 2020;29:102242.
 66. Mathy NL, Scheuer W, Lanzendörfer M, et al. Interleukin-16 stimulates the expression and production of pro-inflammatory cytokines by human monocytes. *Immunology*. 2000;100(1):63-69.
 67. Bellini A, Yoshimura H, Vittori E, Marini M, Mattoli S. Bronchial epithelial cells of patients with asthma release chemoattractant factors for T lymphocytes. *J Allergy Clin Immunol*. 1993;92(3):412-424.
 68. Hessel EM, Cruikshank WW, Van Ark I, et al. Involvement of IL-16 in the induction of airway hyper-responsiveness and up-regulation of IgE in a murine model of allergic asthma. *J Immunol*. 1998;160(6):2998-3005.
 69. Chesné J, Braza F, Mahay G, Brouard S, Aronica M, Magnan A. IL-17 in severe asthma. Where do we stand? *Am J Respir Crit Care Med*. 2014;190(10):1094-1101.
 70. Gee K, Guzzo C, Che Mat NF, Ma W, Kumar A. The IL-12 family of cytokines in infection, inflammation and autoimmune disorders. *Inflamm Allergy Drug Targets*. 2009;8(1):40-52.
 71. Capaldo CT, Nusrat A. Cytokine regulation of tight junctions. *Biochim Biophys Acta Biomembr*. 2009;1788(4):864-871.
 72. Krishn SR, Ganguly K, Kaur S, Batra SK. Ramifications of secreted mucin MUC5AC in malignant journey: A holistic view. *Carcinogenesis*. 2018;39(5):633-651.
 73. Ye X, Sun M. AGR2 ameliorates tumor necrosis factor- α -induced epithelial barrier dysfunction via suppression of NF- κ B p65-mediated MLCK/p-MLC pathway activation. *Int J Mol Med*. 2017;39(5):1206-1214.
 74. Watari A, Sakamoto Y, Hisaie K, et al. Rebeccamycin attenuates TNF- α -induced intestinal epithelial barrier dysfunction by inhibiting myosin light chain kinase production. *Cell Physiol Biochem*. 2017;41(5):1924-1934.
 75. Sorini C, Cosorich I, Lo Conte M, et al. Loss of gut barrier integrity triggers activation of islet-reactive T cells and autoimmune diabetes. *Proc Natl Acad Sci USA*. 2019;116(30):15140-15149.
 76. Youakim A, Ahdieh M. Interferon-gamma decreases barrier function in T84 cells by reducing ZO-1 levels and disrupting apical actin. *Am J Physiol*. 1999;276(5):G1279-G1288.
 77. Willemsen LEM, Hoetjes JP, van Deventer SJH, van Tol EAF. Abrogation of IFN-gamma mediated epithelial barrier disruption by serine protease inhibition. *Clin Exp Immunol*. 2005;142(2):275-284.
 78. Ng CT, Fong LY, Sulaiman MR, et al. Interferon-gamma increases endothelial permeability by causing activation of p38 MAP kinase and actin cytoskeleton alteration. *J Interferon Cytokine Res*. 2015;35(7):513-522.
 79. Smyth D, Phan V, Wang A, McKay DM. Interferon- γ -induced increases in intestinal epithelial macromolecular permeability requires the Src kinase Fyn. *Lab Invest*. 2011;91(5):764-777.

80. Youakim A, Ahdieh M. Interferon- γ decreases barrier function in T84 cells by reducing ZO-1 levels and disrupting apical actin. *Am J Physiol Gastrointest Liver Physiol.* 1999;276(5):G1279-G1288.
81. Scharl M, Paul G, Barrett KE, McCole DF. AMP-activated protein kinase mediates the interferon- γ -induced decrease in intestinal epithelial barrier function. *J Biol Chem.* 2009;284(41):27952-27963.
82. Ozaki H, Ishii K, Horiuchi H, et al. Cutting edge: Combined treatment of TNF- α and IFN- γ causes redistribution of junctional adhesion molecule in human endothelial cells. *J Immunol.* 1999;163(2):553-557.
83. Ordoñez CL, Khashayar R, Wong HH, et al. Mild and moderate asthma is associated with airway goblet cell hyperplasia and abnormalities in mucin gene expression. *Am J Respir Crit Care Med.* 2001;163(2):517-523.
84. Kim S-H, Pei Q-M, Jiang P, et al. Upregulation of MUC5AC by VEGF in human primary bronchial epithelial cells: Implications for asthma. *Respir Res.* 2019;20(1):282.
85. Makinde T, Murphy RF, Agrawal DK. Immunomodulatory role of vascular endothelial growth factor and angiopoietin-1 in airway remodeling. *Curr Mol Med.* 2006;6(8):831-841.
86. Jin W, Dong C. IL-17 cytokines in immunity and inflammation. *Emerg Microb Infect.* 2013;2(9):e60-e60.
87. Deshmane SL, Kremlev S, Amini S, Sawaya BE. Monocyte Chemoattractant Protein-1 (MCP-1): An overview. *J Interferon Cytokine Res.* 2009;29(6):313-326.
88. Bhavsar I, Miller CS, Al-Sabbagh M. Macrophage Inflammatory Protein-1 Alpha (MIP-1 alpha)/CCL3: As a biomarker. In: Preedy VR, Patel VB, eds. *General Methods in Biomarker Research and Their Applications*. London, UK: Springer Netherlands; 2015:223-249.
89. Onishi RM, Gaffen SL. Interleukin-17 and its target genes: Mechanisms of interleukin-17 function in disease. *Immunology.* 2010;129(3):311-321.
90. Cavaillon JM. Pro- versus anti-inflammatory cytokines: Myth or reality. *Cell Mol Biol.* 2001;47(4):695-702.
91. Moser B, Willmann K. Chemokines: Role in inflammation and immune surveillance. *Ann Rheumatic Dis.* 2004;63(Suppl 2):ii84-ii89.
92. Scheffler S, Dieken H, Krischenowski O, Aufderheide M. Cytotoxic evaluation of e-liquid aerosol using different lung-derived cell models. *Int J Environ Res Publ Health.* 2015;12(10):12466-12474.
93. Deschl U, Vogel J, Aufderheide M. Development of an in vitro exposure model for investigating the biological effects of therapeutic aerosols on human cells from the respiratory tract. *Exp Toxicol Pathol.* 2011;63(6):593-598.
94. Steinritz D, Möhle N, Pohl C, et al. Use of the Cultex® radial flow system as an in vitro exposure method to assess acute pulmonary toxicity of fine dusts and nanoparticles with special focus on the intra- and inter-laboratory reproducibility. *Chem Biol Interact.* 2013;206(3):479-490.
95. Wang Y, Wu Q, Muskhelishvili L, Davis K, Bryant M, Cao X. Assessing the respiratory toxicity of dihydroxyacetone using an in vitro human airway epithelial tissue model. *Toxicol In Vitro.* 2019;59:78-86.
96. Fields W, Maione A, Keyser B, Bombick B. Characterization and application of the VITROCELL VC1 smoke exposure system and 3D EpiAirway models for toxicological and e-cigarette evaluations. *Appl In Vitro Toxicol.* 2017;3(1):68-83.
97. Lenz A-G, Stoeger T, Cei D, et al. Efficient bioactive delivery of aerosolized drugs to human pulmonary epithelial cells cultured in air-liquid interface conditions. *Am J Respir Cell Mol Biol.* 2014;51(4):526-535.
98. Diabaté S, Armand L, Murugadoss S, et al. Air-liquid interface exposure of lung epithelial cells to low doses of nanoparticles to assess pulmonary adverse effects. *Nanomaterials.* 2021;11(1):65.
99. Leibrock LB, Jungnickel H, Tentschert J, et al. Parametric optimization of an air-liquid interface system for flow-through inhalation exposure to nanoparticles: Assessing dosimetry and intracellular uptake of CeO(2) nanoparticles. *Nanomaterials.* 2020;10(12):2369.
100. Brandenberger C, Mühlfeld C, Ali Z, et al. Quantitative evaluation of cellular uptake and trafficking of plain and polyethylene glycol-coated gold nanoparticles. *Small.* 2010;6(15):1669-1678.
101. Durantie E, Vanhecke D, Rodriguez-Lorenzo L, et al. Bio-distribution of single and aggregated gold nanoparticles exposed to the human lung epithelial tissue barrier at the air-liquid interface. *Part Fibre Toxicol.* 2017;14(1):49.
102. Brandenberger C, Rothen-Rutishauser B, Mühlfeld C, et al. Effects and uptake of gold nanoparticles deposited at the air-liquid interface of a human epithelial airway model. *Toxicol Appl Pharmacol.* 2010;242(1):56-65.
103. Lenz AG, Karg E, Lentner B, et al. A dose-controlled system for air-liquid interface cell exposure and application to zinc oxide nanoparticles. *Part Fibre Toxicol.* 2009;6:32.
104. Fröhlich E, Bonstingl G, Höfler A, et al. Comparison of two in vitro systems to assess cellular effects of nanoparticles-containing aerosols. *Toxicol In Vitro.* 2013;27(1):409-417.
105. Lenz AG, Stoeger T, Cei D, et al. Efficient bioactive delivery of aerosolized drugs to human pulmonary epithelial cells cultured in air-liquid interface conditions. *Am J Respir Cell Mol Biol.* 2014;51(4):526-535.
106. Loret T, Peyret E, Dubreuil M, et al. Air-liquid interface exposure to aerosols of poorly soluble nanomaterials induces different biological activation levels compared to exposure to suspensions. *Part Fibre Toxicol.* 2016;13(1):58.
107. Korshed P, Li L, Ngo D-T, Wang T. Effect of storage conditions on the long-term stability of bactericidal effects for laser generated silver nanoparticles. *Nanomaterials.* 2018;8(4):218.